



HAL
open science

Influence of the damage generated by abrasive water jet texturing on the tensile static and fatigue behaviour of 3D woven composite in the context of repair

X. Sourd, Redouane Zitoune, Laurent Crouzeix, M. Coulaud, D. Lamouche

► To cite this version:

X. Sourd, Redouane Zitoune, Laurent Crouzeix, M. Coulaud, D. Lamouche. Influence of the damage generated by abrasive water jet texturing on the tensile static and fatigue behaviour of 3D woven composite in the context of repair. *Composites Part A: Applied Science and Manufacturing*, 2021, 149, pp.106567. 10.1016/j.compositesa.2021.106567 . hal-03327314

HAL Id: hal-03327314

<https://hal.science/hal-03327314>

Submitted on 2 Aug 2023

HAL is a multi-disciplinary open access archive for the deposit and dissemination of scientific research documents, whether they are published or not. The documents may come from teaching and research institutions in France or abroad, or from public or private research centers.

L'archive ouverte pluridisciplinaire **HAL**, est destinée au dépôt et à la diffusion de documents scientifiques de niveau recherche, publiés ou non, émanant des établissements d'enseignement et de recherche français ou étrangers, des laboratoires publics ou privés.



Distributed under a Creative Commons Attribution - NonCommercial 4.0 International License

Influence of the damage generated by abrasive water jet texturing on the tensile static and fatigue behaviour of 3D woven composite in the context of repair

X. Sourd^{1,2,*}, R. Zitoune¹, L. Crouzeix¹, M. Coulaud², D. Lamouche²

¹Institut Clément Ader, CNRS UMR 5312, Université Paul Sabatier. 3 Rue Caroline Aigle. 31400 Toulouse, France

²Safran Aircraft Engines (Villaroche). Rond-point René Ravaud. 77550 Moissy-Cramayel, France

* xavier.sourd@iut-tlse3.fr

ABSTRACT

Abrasive water jet (AWJ) process has been certified in some aerospace companies for repair applications. However, there is no information in the literature on the influence of the induced damage on the mechanical behaviour of complex materials such as 3D woven CFRP composite. To fill this gap, three texturing levels have been produced and quantified using both surface roughness (Ra) and “crater volume” (Cv) criteria. The specimens have been subjected to tensile static and tension-tension fatigue tests. Contrarily to Ra measurements, a linear correlation was highlighted between the increase in Cv and the degradation of the specimens’ mechanical performances (ultimate tensile stress and fatigue limit). The damage scenario of the textured specimens has been identified via acoustic emission activity, thermal maps and X-ray tomography pictures. Wider cracks and a more intense acoustic activity leading to a greater rise in temperature have been observed when Cv increases (worse quality). However, the small alterations in mechanical properties consecutive to AWJ texturing prove that this technique can be used for surface preparation of 3D woven CFRP parts prior to bonding without damaging them. Moreover, an innovative method, based on the damage accumulation, has been proposed and accurately estimates the endurance limit of the specimens.

Keywords: Texturing quality, crater volume, tensile behaviour, fatigue

I. Introduction

At a period when air traffic is considerably rising and environmental protection is becoming of primary concern, the aviation industry is subjected to strict regulations to diminish its environmental footprint. To reduce the consumption of their aircraft, manufacturers decided to lighten their structures by introducing advanced materials. In this context, a composite material made of three-dimensional woven

carbon fibres and polymer resin has been designed. This composite material can either be used alone for monolithic parts or combined with another material (e.g. metal) to create hybrid structures. When this material is chosen for the aircraft's outer parts, it may be subjected to damage in flight such as impact or erosion. In this case, and for economic reasons, the repair is favoured to complete replacement of the damaged part. The affected area is then removed by machining (mainly conventional mean) and a patch of new material is applied.

However, it is of common knowledge that Carbon Fibre Reinforced Polymer (CFRP) composite is a difficult to machine material with the conventional process. Indeed, this machining technique induces thermal [1–3] and mechanical damage [1,2,4,5] which are the main causes of degradation of the mechanical performances of the machined parts in service [3,6,7]. Moreover, machining CFRP by conventional means emits fine particles [6,8], harmful to the operators.

Considering these drawbacks and in the scope of counteracting them, the abrasive water jet (AWJ) technique, which is considered a non-conventional process, has recently emerged for repair applications. Indeed, the water flow permits both to neutralize the induced heat and trap the chips and volatile particles of carbon fibres [9,10]. Though the AWJ process has proven to be a suitable machining technique for a large span of materials, from titanium alloy to FRP composite laminates made of unidirectional plies [9,11–14], only a few studies have been conducted on 3D woven composites [15,16]. Thanks to all its advantages over conventional processes, AWJ technique can be considered as an industrial alternative process and even more in the context of composite repair in the aerospace field.

However, as with all material removal processes, AWJ method of CFRP induces several issues. The main problem is surface contamination by abrasive embedment which is not compatible with repairs by adhesive bonding. However, Sourd et al. [16] have shown that very low contamination in 3D woven composite consecutive to AWJ machining can be obtained with the proper selection of process parameters (less than 0,5% of the milled surface). The other types of defects and damage consecutive to AWJ milling of CFRPs are in form of craters, fibre pull-out and fibre-matrix debonding, in addition to delamination in case of machining of laminates [11,16]. As a strong adhesive bonding requires a good surface quality of the two substrates, it is important to quantify these defects and damage and to minimize them. In the industrial field, the main parameter used for surface quality is the Arithmetic average surface roughness (Ra). However, it was shown that this parameter is not suitable to properly describe the quality of AWJ milled surfaces of CFRP laminates (e.g. made of unidirectional plies). To replace Ra, Hejjaji et

al. [11] proposed a new indicator for the quantification of surface quality called crater volume (C_v). It has proven to better correlate the changes in surface quality with the modifications of machining parameters. Indeed, as the jet pressure increases, the available energy within the jet stream transferred to the particles increases, which leads to a harsher erosion of the material than a greater crater volume. Likewise, when the jet exposure time on the workpiece is higher (viz. machining with lower traverse speed and/or smaller scan step) the particles impacting the material are more numerous which induces more craters. The same conclusions have been drawn when performing AWJ milling of 3D woven CFRP composite [16].

As explained by several authors [11,17,18], the changes in the mechanical behaviour of machined specimens (both in static and fatigue) are mainly depending on their surface quality. From an industrial point of view, good machining is currently defined by a low surface roughness (R_a) inducing a small reduction of mechanical performances after machining compared to a pristine structure. However, this correlation is not so obvious and some conclusions in the literature are contradicting. Indeed, Ghidossi et al. [19] have shown that the tensile strength of conventionally milled unidirectional glass fibres / epoxy resin specimens decreased as the surface quality is getting better (i.e. R_a decreases). The opposite conclusions were drawn by Squires et al. [20] who performed compressive tests on unidirectional CFRP coupons after being machined by a conventional process. Similar observations have been made [18,21,22] in the case of compressive tests on AWJ trimmed multidirectional CFRP specimens, with greater compressive strength as the machining quality is improved. On the other hand, a correlation between the AWJ machining quality and the modifications in compressive strength of FRP specimens was found when considering C_v instead of R_a [18]. The comparison of these results tends to prove that the R_a criterion is not a suitable indicator to describe the machining quality of composite materials. It might be even more the case when focusing on 3D woven composites with complex weaving architectures. Once more, the crater volume C_v has proven to be a better indicator of surface quality than classical criterion R_a . Indeed, Hejjaji et al. [11,17] have shown that there is no clear correlation between R_a and the amplitude of drop-in ultimate tensile strength or endurance limit of machined multi-directional CFRP laminates specimens. On the contrary, there is a clear decrease in both ultimate tensile strength and endurance limit as C_v increases. However, to the authors' knowledge, no such results are available concerning 3D woven composites.

The goal of this work is then to analyse the relationship between the surface quality of 3D woven CFRP composite specimens textured by AWJ technique in the context of repair application and their

static (ultimate tensile strength) and fatigue (tension-tension endurance limit) mechanical behaviour. To do so, three levels of surface quality have been generated and quantified through surface roughness (Ra) and “crater volume” (Cv) criteria, both estimated thanks to topologies obtained by 3D optical profilometer scanning. After the characterization phase, tensile static and tension-tension fatigue (stress ratio $R = 0.1$, frequency of 8 Hz) tests have been performed at room temperature. The machined specimens have been multi-instrumented by extensometer and high-speed camera to measure the strains, by acoustic emission transducer in order to detect the damage and follow their evolution and by an infrared camera for the quantification of the warming-up of the specimens consecutive to cyclic loadings.

II. Material and methods

II.1. Material

A plate made of CFRP 3D woven composite has been produced for this study. This material is composed of PR520 (Cytec Company) epoxy resin and IM7 (Hexcel Composites Company) carbon fibres. The process used to manufacture the plate was light Resin Transfer Molding, permitting to obtain a thickness of 11.1 ± 0.04 mm and a nominal fibre volume fraction of around 54%. Being a confidential property of Safran Aircraft Engines (SAE), no further details (e.g. weaving architecture, mechanical properties, etc...) of this material are disclosed.

II.2. Specimens preparation

II.2.1. Abrasive water jet machining

After the de-moulding process, AWJ machine ‘Flow Mach 4c’ (Flow International Corporation), equipped with Hyplex pump and Paser 4 nozzle, was used to perform the specimens’ preparation viz. cutting and texturing. The abrasive selected for the machining operations was Arabian garnet sand in size of 120 mesh supplied by Garnet Arabia Company Ltd (Saudi Arabia). Dog-bone specimens have been cut in the same plate. The machining parameters used for trimming are those recommended by Flow Company. In fact, for the CFRP material, a jet pressure of 360 MPa, an abrasive flow rate of 0.18 kg/min and a standoff distance of 3 mm are used. To analyse the influence of the weaving direction on the mechanical behaviour, two different sets of specimens have been cut, one parallel to the warp direction (later called “warp specimens”), the other parallel to the weft direction (hereafter referred to as “weft

specimens”). The size of the different specimens (cf. Fig. 1) and the test methods followed standards provided by Safran Aircraft Engines. (ASTM standards D3039 for static tensile tests and D3479 for tension-tension fatigue tests respectively).

For the texturing operations, various surface qualities and levels of damage on the specimens have been investigated. To do so, three machining qualities have been tested (cf. Table 1) and referenced under “good”, “medium” and “poor” qualities by using several levels of waterjet pressure (P), jet traverse speed (V), scan step (SS) and standoff distance (SoD). For economic reasons, others machining parameters were maintained constant. The choice of these levels (cf. Table 1) and set values (cf. Table 2) is supported by previous work concerning AWJ milling of 3D woven composite [15,16]. Moreover, an additional constraint linked to the industrial context has to be taken into account. Indeed, in the case of repair application, adhesive bonding requests surface preparation by sandblasting. This operation might be eliminated when machining with AWJ because this process allows generating a textured surface similar to the one obtained by sandblasting process. However, following the recommendations of SAE, the machining depth cannot be greater than 100 μm . By crossing this threshold, the fibres are bared and subjected to damage.

The specimens are screwed on a wooden plate fixed to the machining table to prevent any motion originating from a water swirl during the texturing process. Only one side of the specimens was textured to simulate a repair operation by the AWJ process. The texturing was performed with a raster scan pattern for machining path strategy, with a machining direction maintained parallel to the warp direction (cf. Fig. 2). The path was extended – around 60 mm beyond the ends of the warp specimens and on aluminium masks for the weft specimens –to avoid any instability in traverse speed during the jet direction changes which can lead to over erosion. The textured length of all the specimens was set to 100 mm. For each surface quality and set of specimens (warp and weft), four replicated have been prepared. In addition, four unmachined warp and weft specimens have been investigated to have reference values of ultimate tensile strength and endurance limit.

II.2.2. Machined surfaces and defects characterization

The textured surfaces were characterized by optical profilometer Infinite Focus SL from Alicona. This apparatus uses the focus variation technique to create the profiles and the topographies of the machined surfaces. Table 3 gathers the parameters provided to the profilometer’s software for the profiles and

topographies acquisition. Thanks to the topographies, having an area of 14 mm x 14 mm, it was possible to quantify the amount of damage, mainly in form of craters, consecutive to AWJ texturing. The parameter named “crater volume per unit area” (Cv) has been calculated for all the machined surfaces following the procedure developed in the former study [16].

In order to confirm that the Mean Arithmetic Roughness (Ra) criterion does not correlate with the modifications in the post-machining mechanical behaviour of the specimens, as proven in the literature [11,17,19–22], it has been decided to measure this indicator both on the longitudinal (parallel to machining) and transverse (perpendicular to machining) directions, respectively named Ra_L and Ra_T , from the topographies acquired by an optical profilometer. The conditions of roughness measurement are a cut-off length (sampling length) of 0.8 mm and a total measured length of 14 mm. Each Ra value represents the mean of 5 measurements made along the zone of interest.

II.3. Mechanical characterization and instrumentation

Static tensile and fatigue tensile-tensile tests have been conducted to analyse the influence of the surface quality produced by AWJ texturing on the mechanical behaviour of the machined 3D woven composite specimens. The test methods followed standards provided by Safran Aircraft Engines. (ASTM standards D3039 for static tensile tests and D3479 for tension-tension fatigue tests respectively). As the material is the property of SAE, all the mechanical properties will be standardized by the reference (i.e. non-textured specimens) ones.

II.3.1. Static tensile tests

The static tensile tests were conducted on INSTRON 8800 series servo-hydraulic load frame with a 250 kN load cell. The specimens were subjected to a load piloted by a rate of 2 mm/min until failure. To calculate the ultimate failure stress, the specimens have been submitted to X-Ray tomography to measure the actual area of a cross-section from the images. This permits avoiding errors due to rectangular approximations. The tests were multi-instrumented (cf. Fig. 3) with an extensometer with a gauge length of 50 mm (to measure longitudinal strains) and two acoustic emission wideband transducers (100 kHz – 1 MHz) separated from each other by 70 mm to have the vertical position of the events. In addition, a fine painted speckle pattern has been applied on the textured surface to perform Digital Image Correlation (DIC). The camera used to film the reduced section (14.5 x 70 mm² and 21.5 x 70 mm²) has a resolution

of 15M pixels and the distance from the specimen was around 15 cm. This permits obtaining a spatial resolution under 1 μm , which is within the range of the topological features of the textured surfaces.

II.3.2. Tension-tension fatigue tests

The tension-tension fatigue tests have been performed on the same machine used for the static tests. For the identification of the damage mechanisms, multi-instrumentation by extensometer, acoustic emission transducers and an infrared thermal camera has been performed (cf. Fig. 4). The fatigue tests were designed thanks to the ultimate tensile load values (F_{max}) acquired during the static tensile tests. From these values, the specimens were subjected to 15,000 sinusoidal cycles of tensile-tensile loadings – stress ratio $R = 0.1$ at a frequency of 8 Hz – from 15% F_{max} to 55% F_{max} with an increment of 5% F_{max} at room temperature. Between two consecutive load blocks, a rest time is included to allow the specimens to cool down back to room temperature (from around one minute for 15% F_{max} cycles to 20 minutes for loading blocks close to failure). Fig. 5 shows the loading protocol designed for the tensile-tensile fatigue tests. Three identical tests have been performed for each surface quality and each direction (4 qualities x 2 directions x 3 tests = 24 tests).

The temperature dissipated by the specimens during the fatigue loading has been recorded by a M3K infrared thermal camera (from Telops) with a thermal resolution inferior to 25 mK. The emissivity and image resolution were set to 0.99 and 320×256 pixels respectively. The rise in temperature consecutive to the cycling loadings is used to determine the endurance limit (tension-tension) of the specimens following the temperature stabilization method [17,21,23–25]. This technique is a faster alternative for the estimation of the endurance limit than plotting Whöler curves (stress vs. cycles). The temperature of specimens subjected to cyclic loads rises as the number of cycle increases due to the initiation and propagation of damage (energy irreversibly transformed into heat) until reaching a plateau. The heating-up of the specimen to this stabilized temperature is then plotted with respect to the maximum stress level reached during the block of loading cycles, and this for each load case. The obtained graph can be fitted with two straight lines with different slopes. The intersection of these two lines gives an estimated value of the endurance limit of the specimen. Even though the temperature stabilization method has initially been developed for metallic materials [24,25], some researchers have proven that this technique is suitable for the estimation of the endurance limit of composite specimens [17,21,23].

II.4. Fatigue damage evolution analysis

The evolution of damage within the specimens has been examined thanks to X-ray tomography analysis after being subjected to tensile-tensile loading blocks of 30% F_{\max} and 45% F_{\max} . To do so, EasyTom 130 X-ray tomography machine has been used, with current and voltage of 80 mA and 100 kV respectively. With these parameters, the voxel size (i.e. image resolution) was 16 μm . In addition, the stiffness degradation during cyclic loading is usually used to quantify the damage evolution of composite specimens [23,26] through the damage accumulation (d) following equation (1):

$$d(N) = 1 - \frac{E_N}{E_0} \quad (1)$$

Where $d(N)$ represents the damage accumulation after the N^{th} cycle of the load case.

E_N corresponds to the specimen's stiffness after the N^{th} cycle of the load case.

E_0 corresponds to the initial specimen's stiffness.

The damage accumulation parameter “ d ” will be later used in this study to estimate the endurance limit of the specimens.

III. Results and discussion

Due to the confidentiality of the studied material, all the following results concerning the mechanical behaviour of the specimens are normalized by the values of the reference specimens (i.e. unmachined).

III.1. Material removal and surface quality

The first step before any mechanical test was to characterize the specimens in term of depth of removal and surface quality consecutive to AWJ texturing. Table 4 gathers the values of these features for each set of machining parameters used and for both directions and Fig. 6 shows topographies of the weft specimens for the different machining qualities. Similar depth maps are found for the warp specimens. All the specimens have a depth of removal below or close to 100 μm as recommended by the company (SAE). Of course, the goal of the “poor” quality specimens is to analyse the mechanical behaviour of specimens which depth of removal is very close to the “critical” value. As expected, an increase in crater volume (C_v) has been recorded from “good” to “poor” qualities (+75%), with no influence of the specimen direction. It can be seen that contrarily to C_v criterion, no clear trend can be observed between the different machining qualities when R_a is considered, whatever the measuring direction. Actually, because of the weaving architecture of the 3D woven CFRP specimens, the roughness values are scattered

and depend on both the weaving (warp or weft) and measurement (longitudinal or transverse) directions. This can also be explained by the fact that Ra was initially developed to describe the surface quality of metallic materials, which are homogeneous. Finally, all the specimens are subjected to X-ray tomography after texturing. No cracks originating from the machined surfaces or the cut edges were found (as later shown in Table 7), which is in accordance with previous work [16].

III.2. Static tensile behaviour

The stress-strain curves of the different “warp” and “weft” specimens are presented in Fig. 7. The “good” quality “warp” specimen has similar tensile behaviour to the reference one, with linear elastic behaviour and brittle fracture. On the contrary, both “medium” and “poor” specimens present non-linear behaviour (noted Zone 2) before failure, probably due to the greater machine induced damage, leading to a loss of stiffness (cf. Fig. 7a). However, as seen from Fig. 7b, the behaviour of the “weft” specimens is very different from the “warp” specimens and less dependent on the machining quality. Indeed, all the “weft” specimens present an initial linear elastic behaviour (noted Zone 1) similar to the one observed on “warp” specimens but a more pronounced non-linear behaviour part. It can also be noticed that “warp” specimens present a shorter linear elastic zone, a lower strength but a greater strain to failure compared to “warp” specimens. These two tensile behaviours are in accordance with the work of Warren et al. [27] on 3D woven CFRP composite. The authors attributed this difference in tensile behaviour to the greater level of a crimp in the weft direction than in the warp direction.

But, despite these different behaviours, the Young modulus of all the machined specimens is very similar to the reference ones’, with around 7% of the difference between reference and “poor” quality specimens (cf. Fig. 8). This might mean that the presence of craters on the machined surfaces does not affect the mechanical behaviour of the specimens at low load levels (Zone 1 in the stress-strain curves).

When focusing on the ultimate tensile strength σ_{\max} as a function of the machining quality defined by Ra (as usual in the industrial context), the resulting trends are very different depending on the direction of measurement. Indeed, when roughness is measured parallel to the machining direction (i.e. Ra_L , cf. Fig. 9a), no correlation was found between the increase in Ra_L and the decrease in σ_{\max} . This is because Ra_L describes the quality of one jet pass, both machining and measuring directions being parallel. Moreover, a clear distinction is seen from the “warp” and “weft” specimens’ values of Ra_L , showing that this parameter depends on the measuring direction. On the contrary, a clear linear correlation can be

observed when analysing the evolution of σ_{\max} as a function of Ra_T (measuring direction perpendicular to the machining direction, cf. Fig. 9b). Indeed, an increase in Ra_T from 6.37 to 9.50 μm leads to a decrease of almost 15% in σ_{\max} . This can be explained by the fact that Ra_T better describes the surface quality of the machined surfaces. Measuring Ra perpendicular to the machining direction permits capturing the changes in topology induced by the consecutive passes constitutive of the texturing path. This is in accordance with the work of Hejjaji et al. [11] on AWJ machining of CFRP composite laminates made of unidirectional plies. Indeed, the authors highlighted ridges parallel to the machining direction, then induced by the consecutive jet passes, on the surface when milling was performed with a scan step of 1.5 mm. However, Ra_T is very dependent on the weaving architecture, which can be concluded from the difference in Ra_T values for the same machining quality both on warp and weft direction. For example, “good” machining quality leads to a transverse roughness of 6.37 and 8.32 μm for warp and weft specimens respectively, hence a difference of 30%. These various trends tend to prove that Ra cannot be considered as a reliable machining quality criterion to describe 3D woven composite machined surfaces. However, a clearer linear correlation can be seen for both groups of specimens when considering the Crater Volume C_v as machining quality criterion (cf. Fig. 9c). Indeed, a decrease in σ_{\max} is observed when C_v increases (-10% in σ_{\max} when C_v goes from 1.02 to 1.91 mm^3/cm^2 for “weft” specimens). This trend is similar to the conclusions drawn by Hejjaji et al. [17] in the case of AWJ milling of CFRP laminates made of unidirectional plies or Nguyen-Dinh et al. [18] in case of conventional edge trimming of CFRP laminates made of unidirectional plies. Moreover, though the values of the ultimate tensile strength consecutive to the different machining qualities are close from each other, the influence of C_v is slightly greater for the “weft” specimens (-10% in σ_{\max} between “good” and “poor” qualities against -7% in σ_{\max} for “warp” specimens). Though the ultimate tensile strength of the “good” and “medium” quality “weft” specimens seems to be greater than the reference value (respectively +8% and +6%), the difference is too small to conclude that machining improves the tensile static behaviour of the specimens.

The effect of the craters induced by AWJ machining on the specimens’ tensile mechanical behaviour is confirmed by the analysis of the longitudinal strain maps obtained by DIC (cf. Table 5). The focus is made on the distribution of the strains throughout the surface rather than their amplitudes. At first, under low tensile load, machining does not impact the strains distribution which is piloted by the weaving architecture of the composite. This is in accordance with the stress-strain curves and Young moduli presented in Fig. 7. However, as the tensile load increases until reaching failure, the influence of the

machining quality intervenes in the strains distribution and highly localised tensile strains are observed on the “poor” quality specimens, where craters are the deeper (arrow on the bottom right picture in Table 5).

To complete the analysis of the tensile static tests, the damage scenarios of all the specimens have been studied via the recorded acoustic activity. It can be seen from Fig. 10 that as the crater volume increases (i.e. as the machining quality worsen), the stress amplitude inducing the first crack (i.e. the beginning of acoustic activity) is greater. As seen from Fig. 10a, the stress amplitude of first crack goes from around 22% to 36% of σ_{\max} for reference and poor machining quality specimens respectively. Moreover, this result is independent of the loading direction (warp or weft). By analysing the evolution of the acoustic activity during the loadings, it was found that the energy released at the first acoustic event increases as the surface quality worsens. Indeed, the released energy is similar for reference and “good” quality specimens, for both warp and weft directions. However, the acoustic energy is 150 times greater for “poor” quality specimens. This tends to prove that the first crack occurs within the matrix for reference and “good” quality specimens, needing a small load and releasing little energy. On the contrary, as the resin rich layer is almost entirely machined for “poor” quality specimens, the fibres are directly subjected to the loads and fail at greater loads and release a higher amount of energy. In addition, the evolution in acoustic energy released by the cracks can be linked to the trends observed on the stress-strain curves, especially for the “weft” specimens. Indeed, as seen from Fig. 10b, the reduction in stiffness on the stress-strain curve corresponds to the duration of intense acoustic activity (red zone). This confirms that the loss of stiffness is mainly due to fibre cracking which dissipates a huge amount of energy compared to matrix or fibre/matrix interface cracking. Similar observations can be made for the other “weft” specimens. High matrix cracking and fiber/matrix debonding leading to fibre failure have been also noticed in the work of Warren et al. [27] during the transition between zones 1 and 2 noticed in the stress-strain curves. However, no such conclusion can be drawn for the “warp” specimens. This can be explained by the fact that the non-linear behaviour part on the “warp” specimens’ stress-strain curves is less discernible than for the “weft” specimens.

Despite these results, the main conclusion to draw from the analysis of the tensile tests is that the machining quality, i.e. the amount of Cv, following the recommendations described in section II.2.1, has no significant effect on the mechanical behaviour of the specimens. Indeed, differences between reference and “poor” quality specimens are below 10%. To complete the study, a similar analysis has to be made in the case of tension-tension fatigue tests.

III.3. Tension-tension fatigue behaviour

The evolution of the endurance limit has been estimated for all the specimens thanks to the temperature stabilization method, as described in section II.3.2, and correlated to the surface quality, at first defined by mean arithmetic surface roughness R_a in both directions. As seen in Fig. 11a and b, there is no clear correlation between the loss of endurance limit and the evolution of R_{aL} or R_{aT} . This observation definitively proves that R_a is not suitable to describe the quality of 3D woven composite AWJ textured surfaces. However, when plotting the loss of endurance limit as a function of C_v (cf. Fig. 11c), a linear correlation can be found. Indeed, as C_v increases from $1 \text{ mm}^3/\text{cm}^2$ (“good” quality specimens) to $2 \text{ mm}^3/\text{cm}^2$ (“poor” quality specimens), the drop in endurance limit compared to the reference specimens goes from around -3% to -10%. Moreover, the evolution in endurance limit with respect to the surface quality defined by C_v seems to be independent of the weaving direction, which is not the case with R_a . This can be explained by the fact that R_a is an average measurement and local damage such as crater is underestimated. The clear relationship between the endurance limit and C_v might mean that the local damage is driven by the crater dimensions which weaken the specimens. Similar results have been presented by Hejjaji et al. [17] in the case of AWJ milling of CFRP laminates made of unidirectional plies.

The analysis of the thermal maps in Table 6 confirms this hypothesis. Indeed, a greater rise in temperature can be observed on the specimens, in both loading directions, as the machining quality worsens for the same stress amplitude. This could be due to the greater amount of cracks within the matrix and tows which eases friction, hence increases the general temperature of the specimens in the loading area. This assumption is supported by the work of Song et al. [28]. Indeed, the authors performed weft direction tension-tension fatigue tests on pristine (untextured) 3D woven CFRP composites and showed that weft tows first rotate, enhancing their mechanical performances. If this enhancement is not sufficient, progressive damage occurs in form of matrix and tows failure. In the case of textured specimens, the outmost resin layer is finer, which eases matrix cracking when the tows rotate. The analysis of the X-tomography pictures in Table 7 permit to specify the damage scenario of the different “warp” specimens. The pictures in the first row show that almost no damage occur in the specimens at least after the 30% F_{max} load block. However, several cracks at the interface between the fibres and the matrix are observed inside the specimens after the 45% F_{max} load block. Though the crack density seems

to be similar for both “good” and “poor” machining qualities specimens, “poor” quality specimen’s cracks appear to be wider than the “good” quality specimen’s ones. This can be explained by the fact that they appear sooner and then are subjected to a greater number of cycles, which widen them. This assumption is supported by the observation of the bottom left corner crack on the “poor” quality specimen in Table 7.

To complete the analysis of the fatigue tests, the evolution of the damage within the specimens through the different loading blocks is studied thanks to the damage accumulation d , as defined in section II.4. Fig. 12 shows the evolution of d through the different cyclic loading blocks (via normalized cycles N/N_f) for a warp specimen machined with “good” quality. It can be seen that, for loads below 35% of the ultimate tensile load F_{max} , almost no damage is recorded in the specimen (d below 1%). This is confirmed by the tomography pictures in Table 7. When using higher loads, damage slowly increases (from 35% to mid-55% F_{max} loads in Fig. 12) until reaching a critical point where d intensifies drastically within few cycles until failure of the specimen (end of 55% F_{max} curve in Fig. 12). Similar curves are found for all the specimens. These observations are in accordance with other works [23,26] studying fatigue damage in CFRP laminates made of unidirectional plies.

The endurance limit is by definition the stress level below which a specimen can withstand two million cycles without exhibiting any fatigue failure. Hence, the analysis of the damage accumulation evolution as a function of the applied stress might permit to estimate the fatigue limit. Indeed, as already explained previously, there is a threshold value of stress below which no damage is recorded and above which damage increases rapidly as the applied stress increases. Following a methodology similar to the one described in section II.3.2 for the Temperature Stabilization Method (TSM), the endurance limit has been estimated for all the tested specimens. This evaluation technique, using the evolution of the damage accumulation as a function of the applied stress of the cyclic loading block and presented in Fig. 13a, has been named Damage Accumulation Method (DAM). It can be concluded that damage accumulation d and temperature have extremely close trends throughout the loading protocol. This is in accordance with the work of Saleem et al. [23] who have highlight similar evolution for the temperature and the damage accumulation when the number of loading cycles increases in case of tension-tension fatigue tests of composite laminates made of unidirectional CFRP plies with circular holes performed by AWJ machining. The values of endurance limit obtained thanks to DAM are then extremely close to the ones estimated by TSM, with a relative difference between the two methods below 6.5% as seen from Fig. 13b.

These results tend to prove that the Damage Accumulation Method is a suitable alternative to the Temperature Stabilization Method to estimate the endurance limit of the specimens. Moreover, the main advantage of DAM is economical which could be of primary concern both in the research and industrial fields. Indeed, it only requires an extensometer to obtain the longitudinal strains and hence determine the specimen's stiffness for all the different loading cycles against an expensive infrared camera for TSM.

IV. Conclusion

The goal of this study was to analyse the influence of post-AWJ texturing surface quality of 3D woven CFRP composite specimens on their static (ultimate tensile strength) and fatigue (tension-tension endurance limit) mechanical behaviour. Based on the results presented in this work, the following conclusions can be drawn:

- Mean arithmetic surface roughness Ra, usually used in the industrial field to describe the surface texture, has proven to be unsuitable to correlate the surface quality of AWJ textured 3D interlock woven CFRP composite specimens and the modifications in their tensile behaviour both under static (ultimate tensile strength) and fatigue (endurance limit) loadings.
- “Crater volume” criterion, which has been established as a better indicator than Ra for textured surfaces [11,16], highlights the relationship between the worsening of machining quality and the deterioration of the mechanical properties both static and fatigue and for both warp and weft loading directions, even for low variations. Indeed, drops of 4% and 10% in endurance limit compared to as-received specimens are observed for coupons which surface quality, defined by Cv criterion, are respectively $1 \text{ mm}^3/\text{cm}^2$ and $2 \text{ mm}^3/\text{cm}^2$.
- An innovative methodology, called Damage Accumulation Method (DAM), has been proposed to estimate the endurance limit of the specimens through the analysis of the damage accumulation. This technique has shown relevant results in accordance with the ones obtained by Temperature Stabilization Method which is a well-established technique. Moreover, DAM has an economical advantage over TSM as it only needs an extensometer, against an expensive infrared camera for TSM.
- Finally, this study permitted to confirm that the mechanical properties are similar between non-textured and textured specimens which depth of removal is below $100 \text{ }\mu\text{m}$, as recommended by SAE in the context of repair. Indeed, a difference inferior to 10% has been found between reference (non-

textured) and “poor” quality (high craters) specimens on both loading directions and both for the ultimate tensile strength and the endurance limit.

Acknowledgments

The collaboration with Safran Aircraft Engines is gratefully acknowledged.

References

- [1] König W, Wulf C, Grass P, Willerscheid H. Machining of Fibre Reinforced Plastics. *Ann CIRP* 1985;34:537–48.
- [2] Nguyen-Dinh N, Hejjaji A, Zitoune R, Bouvet C, Crouzeix L. Machining of FRP Composites: Surface Quality, Damage, and Material Integrity: Critical Review and Analysis. *Futur. Compos.*, 2018.
- [3] Nguyen-Dinh N, Zitoune R, Bouvet C, Le Roux S. Surface integrity while trimming of composite structures: X-ray tomography analysis. *Compos Struct* 2019;210:735–46.
- [4] Koplev A, Lystrup A, Vorm T. The cutting process, chips, and cutting forces in machining CFRP. *Composites* 1983;14:371–6.
- [5] Voss R, Seeholzer L, Kuster F, Wegener K. Influence of fibre orientation, tool geometry and process parameters on surface quality in milling of CFRP. *CIRP J Manuf Sci Technol* 2017;18:75–91.
- [6] Haddad M, Zitoune R, Eyma F, Castanié B. Study of the surface defects and dust generated during trimming of CFRP: Influence of tool geometry, machining parameters and cutting speed range. *Compos Part A Appl Sci Manuf* 2014;66:142–54.
- [7] Haddad M, Zitoune R, Eyma F, Castanié B. Influence of Machining Process and Machining Induced Surface Roughness on Mechanical Properties of Continuous Fiber Composites. *Exp Mech* 2014;55:519–28.
- [8] Ramulu M, Kramlich J. Machining of fiber reinforced composites: Review of environmental and health effects. *Int J Environ Conscious Des Manuf* 2004;11:1–19.
- [9] Hashish M. An Investigation of Milling With Abrasive-Waterjets. *J Eng Ind* 1989;111:158.
- [10] Ramulu M, Kunaporn S, Arola D, Hashish M, Hopkins J. Waterjet Machining and Peening of Metals. *Analyzer* 2000;122:90–5.
- [11] Hejjaji A, Zitoune R, Crouzeix L, Le Roux S, Collombet F. Surface and machining induced damage characterization of abrasive water jet milled carbon/epoxy composite specimens and their impact on tensile behavior. *Wear* 2017;376–377:1356–64.
- [12] Arola D, Ramulu M. Material removal in abrasive waterjet machining of metals - Surface integrity and texture. *Wear* 1997;210:50–8.
- [13] Hashish M. Waterjet Machining of Advanced Composites. *Mater Manuf Process* 1995;10:1129–52.
- [14] Hejjaji A, Zitoune R, Crouzeix L, Collombet F, Le Roux S. Impact of the abrasive water jet milling process on the damage and surface characteristics of CFRP composite. *ECCM 2016 - Proceeding 17th Eur Conf Compos Mater* 2016.
- [15] Sourd X, Zitoune R, Crouzeix L, Salem M, Charlas M. New model for the prediction of the machining depth during milling of 3D woven composite using abrasive waterjet process. *Compos Struct* 2020;234.
- [16] Sourd X, Zitoune R, Hejjaji A, Salem M, Crouzeix L, Lamouche D. Multi-scale analysis of the generated damage when machining pockets of 3D woven composite for repair applications using abrasive water jet process: Contamination analysis. *Compos Part A Appl Sci Manuf* 2020;139:106118.
- [17] Hejjaji A, Zitoune R, Toubal L, Crouzeix L, Collombet F. Influence of controlled depth abrasive water jet milling on the fatigue behavior of carbon/epoxy composites. *Compos Part A Appl Sci Manuf* 2019;121:397–410.
- [18] Nguyen-Dinh N, Bouvet C, Zitoune R. Influence of machining damage generated during trimming of CFRP composite on the compressive strength. *J Compos Mater* 2019.

- [19] Ghidossi P, El Mansori M, Pierron F. Edge machining effects on the failure of polymer matrix composite coupons. *Compos Part A Appl Sci Manuf* 2004;35:989–99.
- [20] Squires CA, Netting KH, Chambers AR. Understanding the factors affecting the compressive testing of unidirectional carbon fibre composites. *Compos Part B Eng* 2007;38:481–7.
- [21] Haddad M, Zitoune R, Bougherara H, Eyma F, Castanié B. Study of trimming damages of CFRP structures in function of the machining processes and their impact on the mechanical behavior. *Compos Part B Eng* 2014;57:136–43.
- [22] Ramulu M, Colligan K. Edge finishing and delamination effects induced during abrasive waterjet machining on the compression strength of a graphite/epoxy composite. *Am Soc Mech Eng Mater Div MD* 2005;100 MD:173–9.
- [23] Saleem M, Toubal L, Zitoune R, Bougherara H. Investigating the effect of machining processes on the mechanical behavior of composite plates with circular holes. *Compos Part A Appl Sci Manuf* 2013;55:169–77.
- [24] La Rosa G, Risitano A. Thermographic methodology for rapid determination of the fatigue limit of materials and mechanical components. *Int J Fatigue* 2000;22:65–73.
- [25] Luong MP. Fatigue limit evaluation of metals using an infrared thermographic technique. *Mech Mater* 1998;28:155–63.
- [26] Saleem M, Zitoune R, El Sawi I, Bougherara H. Role of the surface quality on the mechanical behavior of CFRP bolted composite joints. *Int J Fatigue* 2015;80:246–56.
- [27] Warren KC, Lopez-Anido RA, Goering J. Experimental investigation of three-dimensional woven composites. *Compos Part A Appl Sci Manuf* 2015;73:242–59.
- [28] Song J, Wen W, Cui H, Li L. Weft direction tension-tension fatigue responses of layer-to-layer 3D angle-interlock woven composites at room and elevated temperatures. *Int J Fatigue* 2020;139:105770.

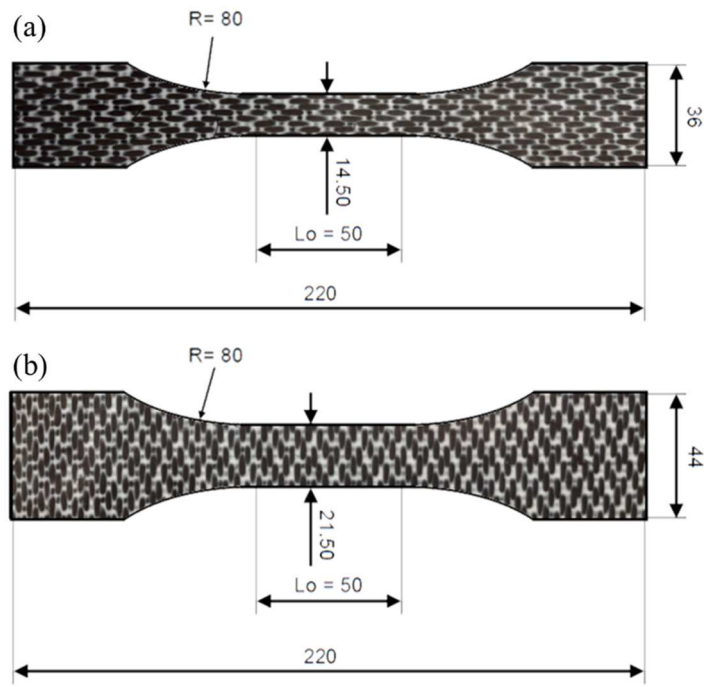


Fig. 1 Geometry of the “warp” (a) and “weft” (b) specimens. The thickness is 11 mm.

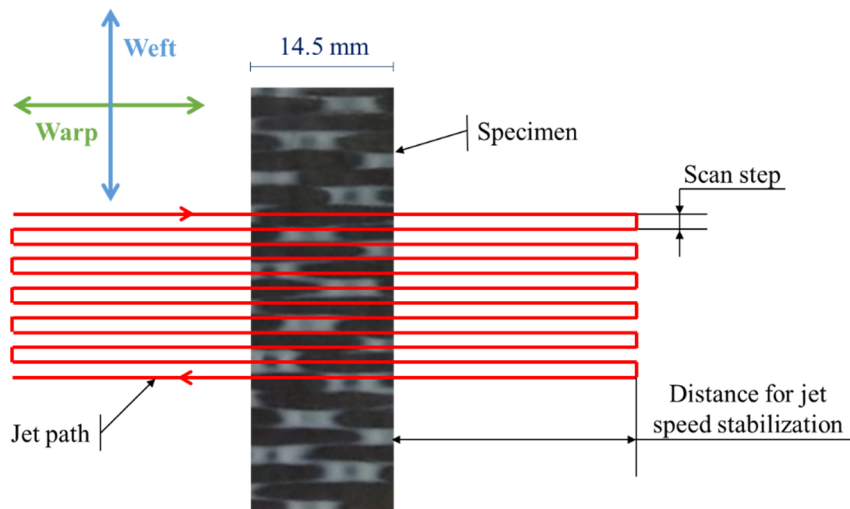


Fig. 2 Schematic view of the milling path strategy.

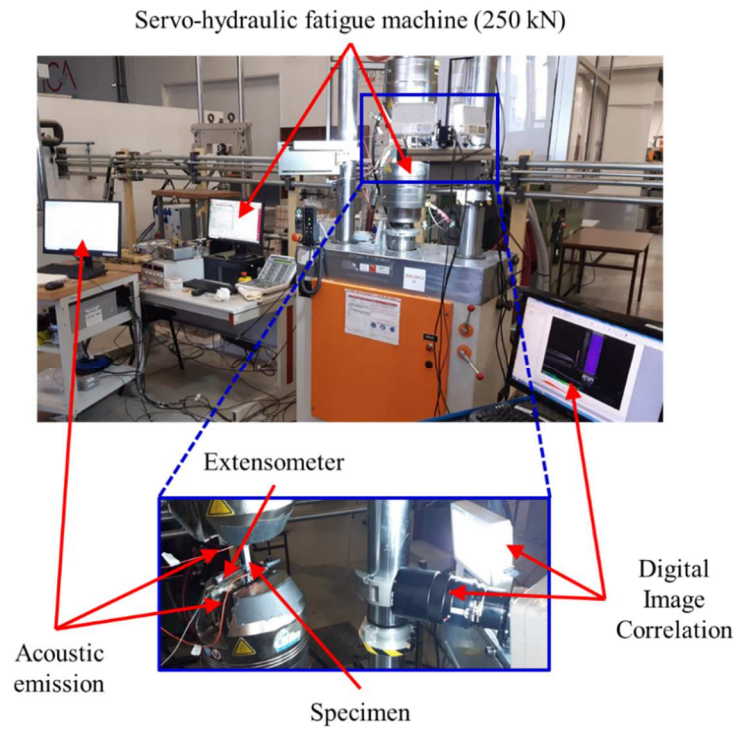


Fig. 3 Experimental setup with the multi-instrumentation used for the tensile static tests.

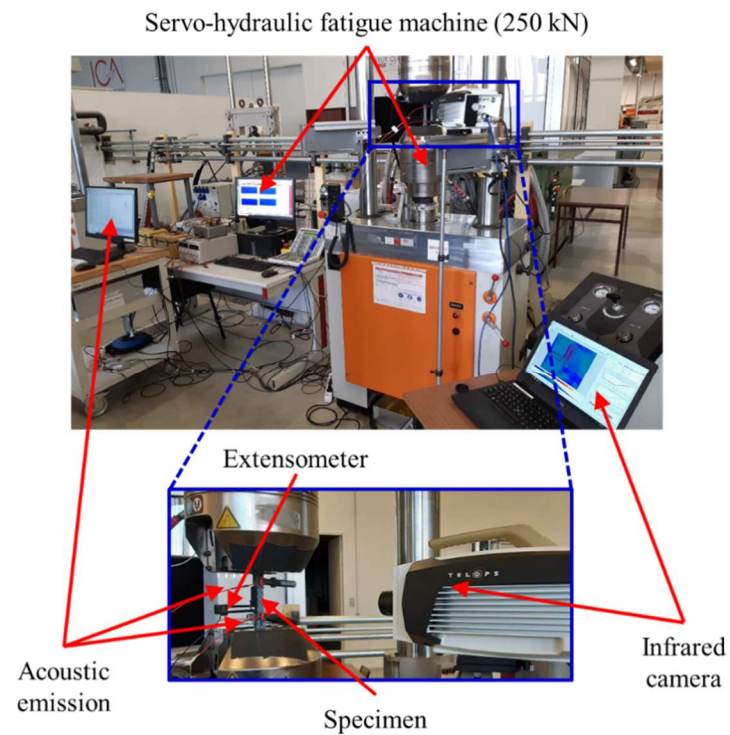


Fig. 4 Experimental setup used for the tension-tension fatigue static tests.

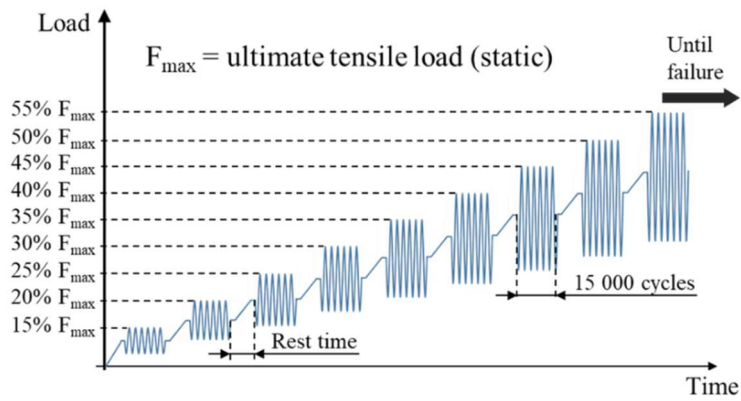


Fig. 5 Tension-tension fatigue tests loading protocol.

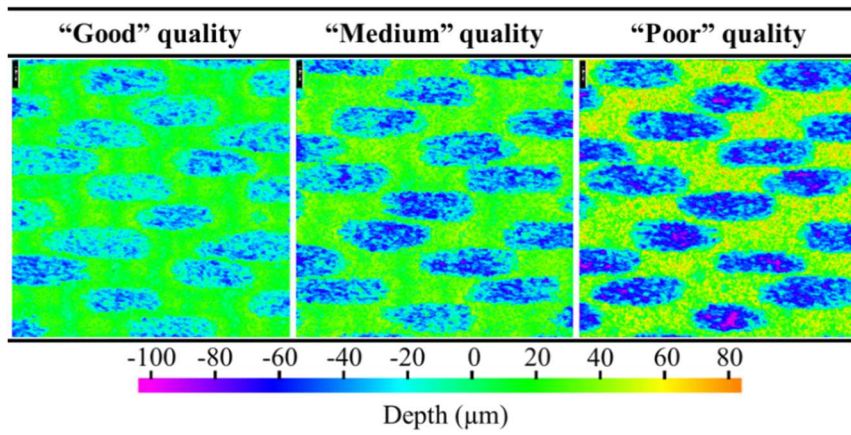


Fig. 6 Topographies of the weft specimens for different machining qualities (2 x 2 cm²).

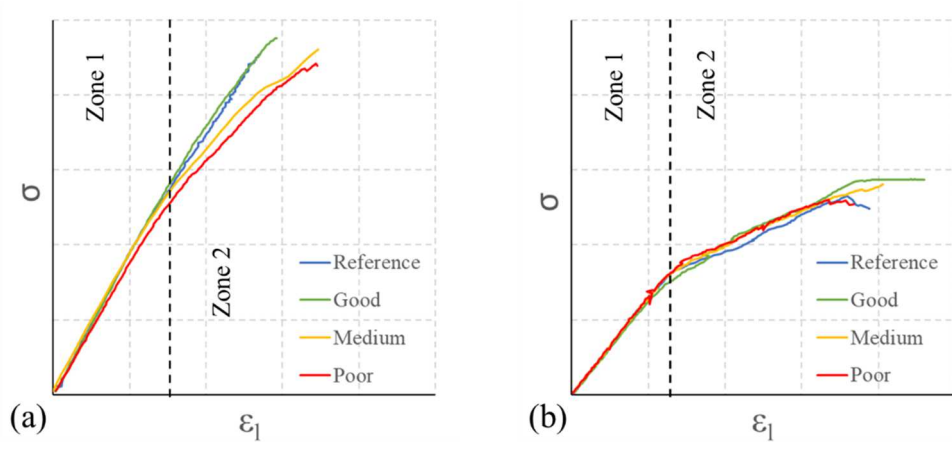


Fig. 7 (a) Standardized stress-strain curves of the different “warp” and (b) “weft” specimens.

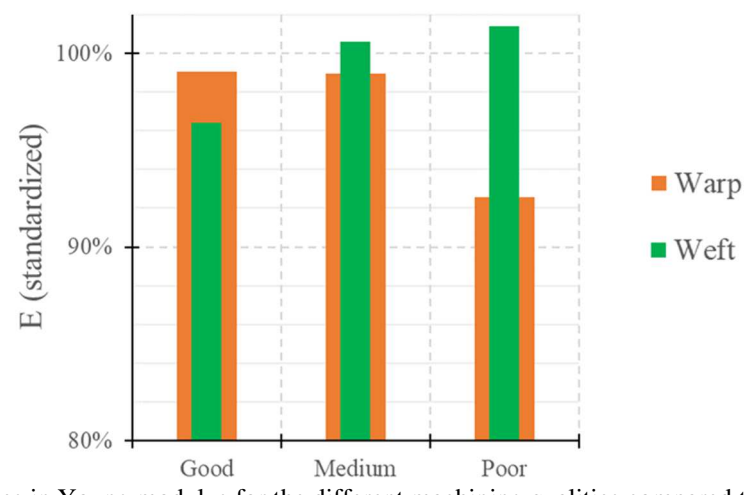


Fig. 8 Changes in Young modulus for the different machining qualities compared to the reference specimens.

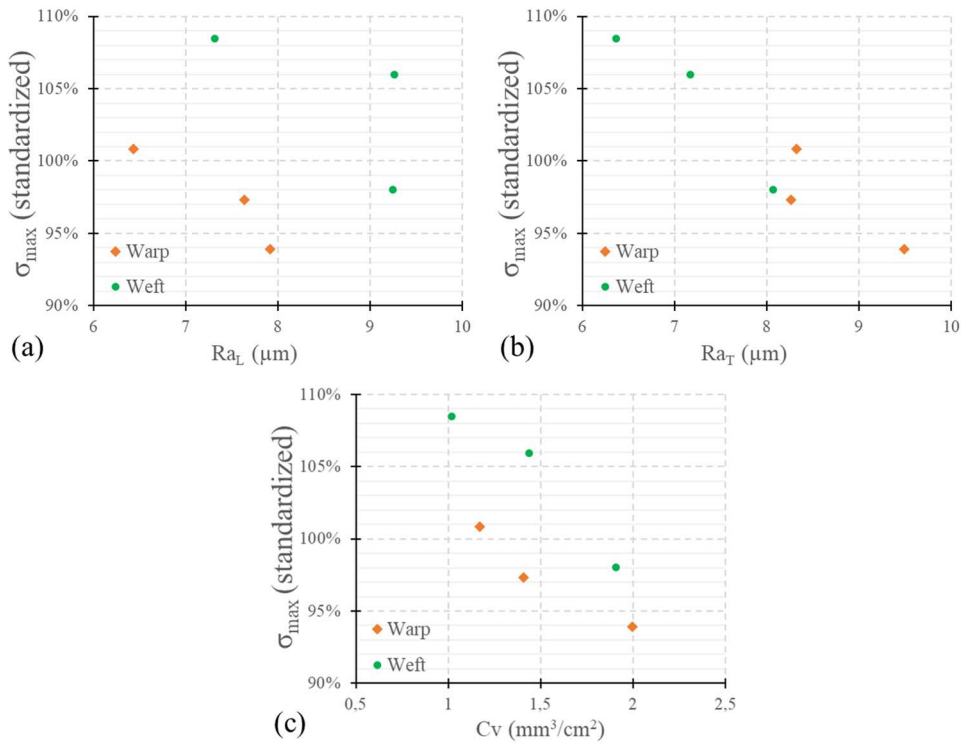


Fig. 9 Standardized evolution of the ultimate tensile strength σ_{max} as a function of the Mean Arithmetic Roughnesses Ra_L (a) and Ra_T (b) and the crater volume Cv (c).

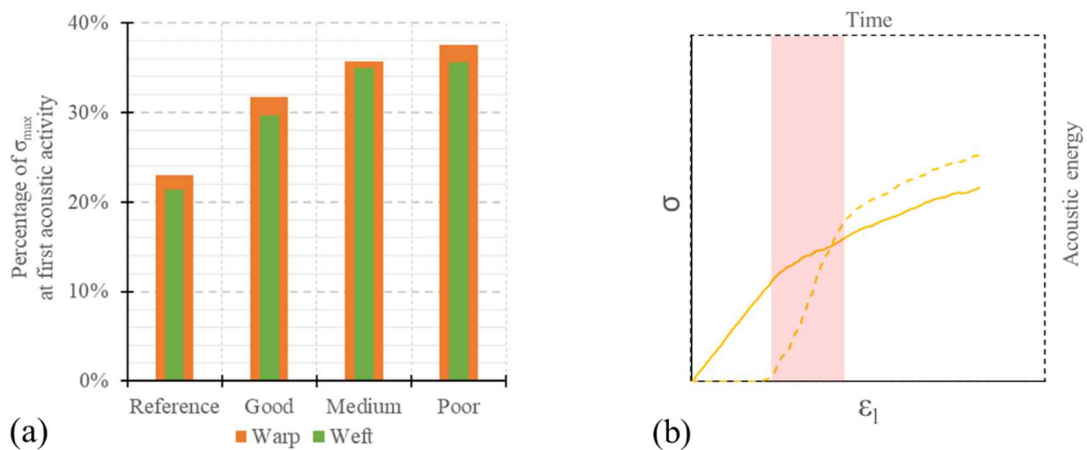


Fig. 10 Acoustic emission activity during loading, with: (a) the evolution of the percentage of ultimate tensile strength (σ_{max}) at first acoustic activity for all the tested specimens and (b) the correlation between the acoustic activity (dotted curve) and the evolution in stiffness (continuous curve) for the weft "medium" quality specimen.

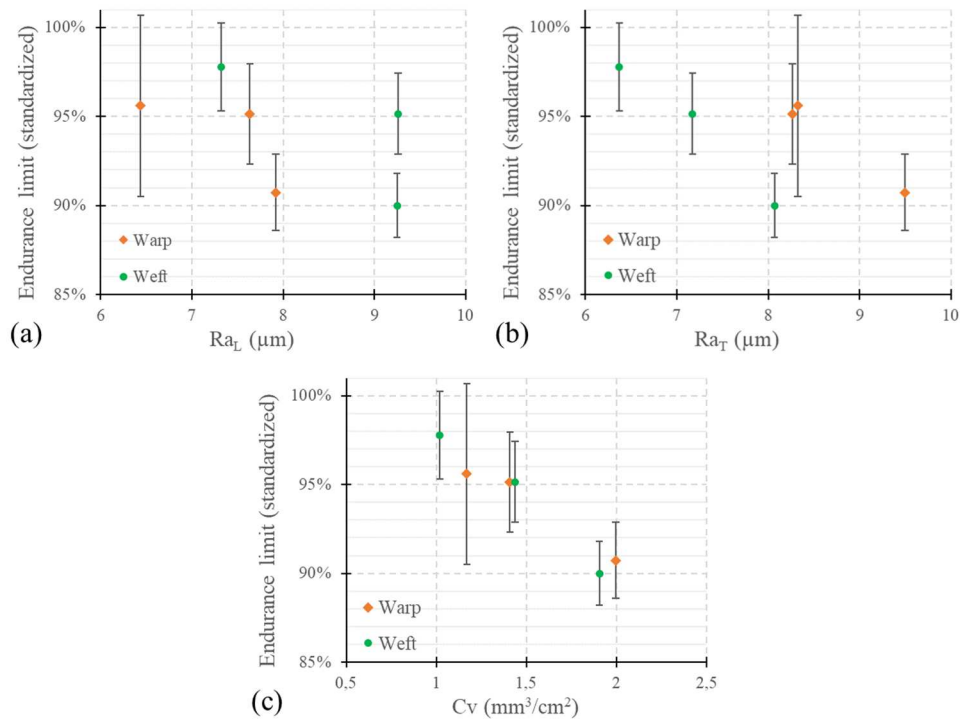


Fig. 11 Standardized evolution of the endurance limit as a function of (a) the Mean Arithmetic Roughnesses Ra_L (a) and Ra_T (b) and the crater volume Cv (c).

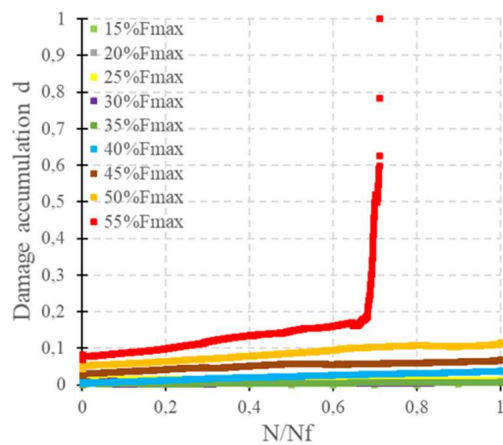


Fig. 12 Evolution of the damage accumulation through the different loading blocks (warp “good” quality specimen).

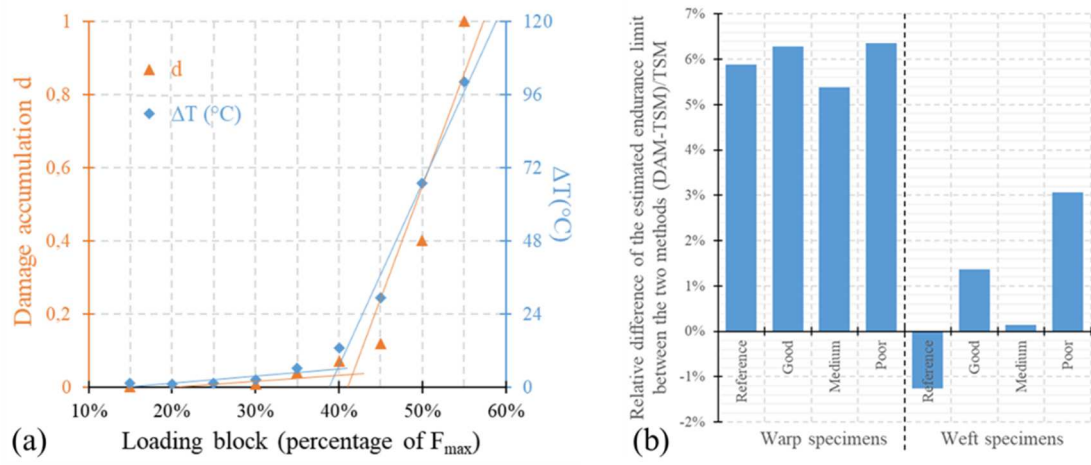


Fig. 13 Damage evolution at the end of the cycle loading vs. the percentage of the applied load, with: (a) example of endurance limit estimation with DAM and TSM methods and (b) comparison of the results obtained by the two techniques.

Table 1: Variable parameters selected for the milling operations to generate several surface qualities.

Parameter	Good	Value Medium	Poor
Pressure P (MPa)	35	35	45
Traverse speed V (m/min)	16	14	14
Scan step SS (mm)	1.75	1.75	1.5
Standoff distance SoD (mm)	150	100	100

Table 2 Set parameters selected for all the milling operations.

Parameter	Value
Focusing tube diameter	1.016 mm
Focusing tube length	76 mm
Nozzle diameter	0.3302 mm
Type of abrasive	Garnet sand
Abrasive size	#120
Abrasive flow rate	0.18 kg/min

Table 3 Parameters selected for the profiles and topographies acquisition.

Parameter	Value
Objective	10x
Vertical resolution (μm)	0.4
Lateral resolution (μm)	< 8

Table 4 Mean values of depth of removal (H), crater volume (Cv) and longitudinal and transverse surface roughness (Ra_L and Ra_T) of the different specimens consecutive to AWJ texturing.

Direction	Quality	H (μm)	Cv (mm^3/cm^2)	Ra_L (μm)	Ra_T (μm)
Warp	Good	66	1.17	6.44	8.32
	Medium	75	1.41	7.64	8.27
	Poor	98	2.00	7.92	9.50
Weft	Good	70	1.02	7.32	6.37
	Medium	74	1.44	9.26	7.17
	Poor	104	1.91	9.25	8.07

Table 5 Longitudinal strain maps of “weft” non-machined and with “poor” machining quality specimens under low and high tensile loads. Arrows show the strain concentration zones.

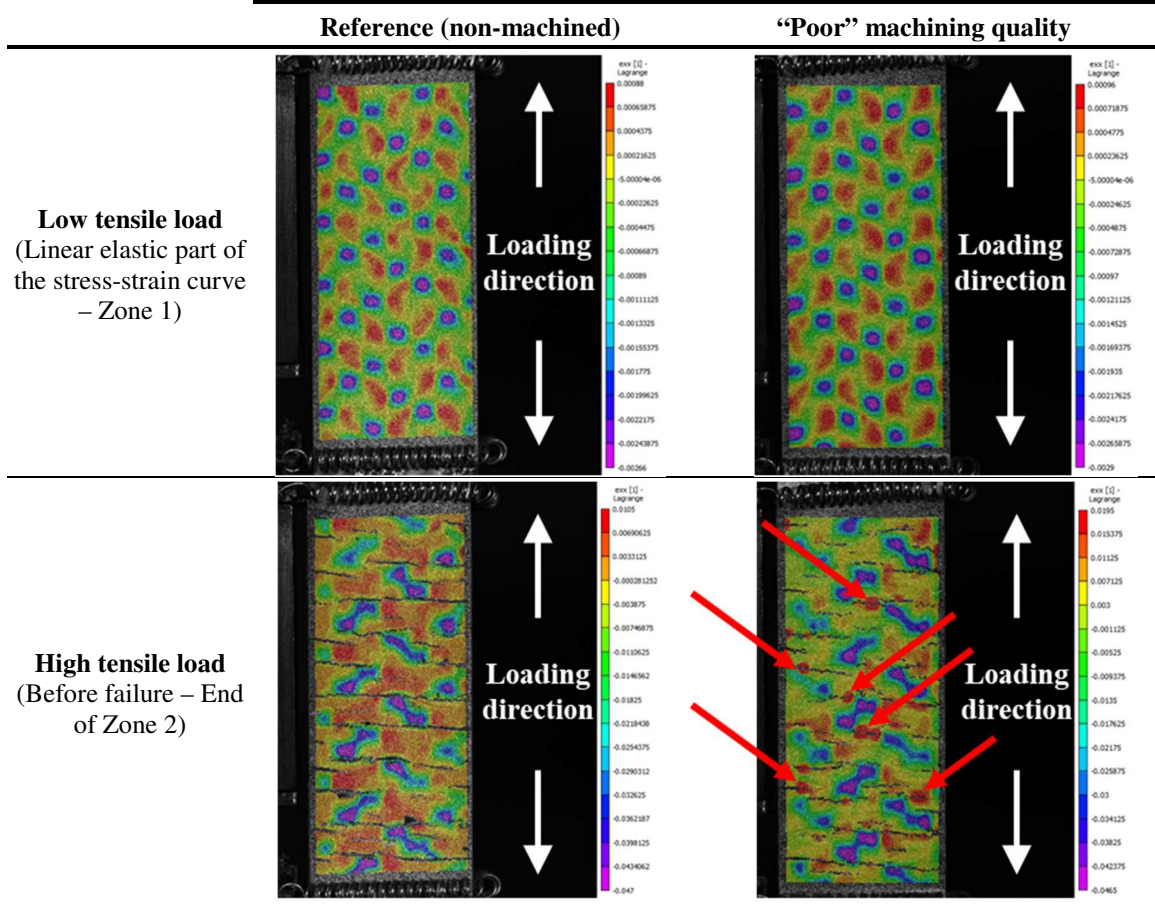


Table 6 Thermal maps of warp and weft specimens for similar stress amplitude ($50\% \sigma_{max}$).

Reference (non-	“Good”	“Medium”	“Poor”
-----------------	--------	----------	--------

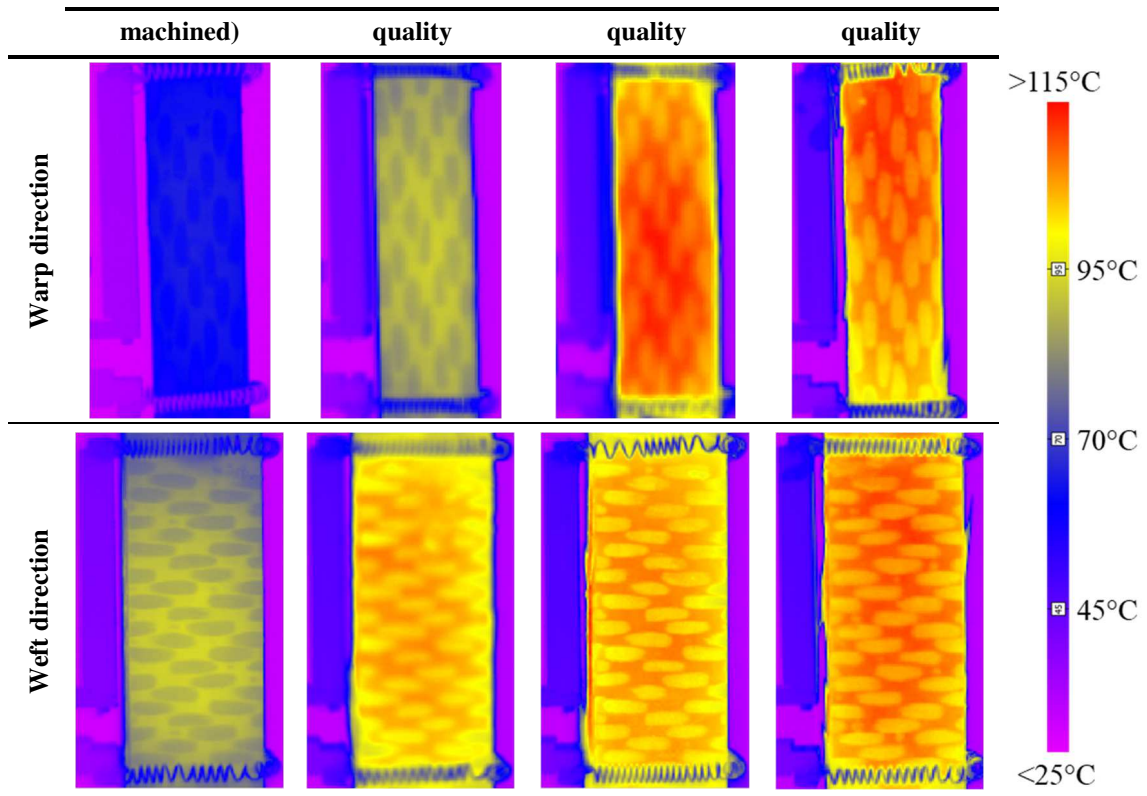


Table 7 Evolution of cracks thanks to cross section X-Ray tomography pictures of “warp” specimens after 30% F_{max} and 45% F_{max} cyclic loading blocks for “good” and “poor” machining qualities.

